BIOCHEMISTRY
including biophysical chemistry & molecular biology

Accelerated Publication

pubs.acs.org/biochemistry

Expression, Purification, Characterization, and Solution Nuclear Magnetic Resonance Study of Highly Deuterated Yeast Cytochrome *c* Peroxidase with Enhanced Solubility

Alexander N. Volkov,*[,†,‡] Alexandre Wohlkonig,[§] Sameh H. Soror,[§,∥] and Nico A. J. van Nuland[†,‡]

[†]Jean Jeener NMR Centre, Structural Biology Brussels, Vrije Universiteit Brussel, Pleinlaan 2, 1050 Brussels, Belgium

[‡]Molecular Recognition Unit, Department of Structural Biology, VIB, Pleinlaan 2, 1050 Brussels, Belgium

[§]JAST lab, Department of Structural Biology, VIB, Pleinlaan 2, 1050 Brussels, Belgium

[∥]Department of Biochemistry and Molecular Biology, Faculty of Pharmacy, Helwan University, Cairo, Egypt

Supporting Information

ABSTRACT: Here we present the preparation, biophysical characterization, and nuclear magnetic resonance (NMR) spectroscopy study of yeast cytochrome *c* peroxidase (CcP) constructs with enhanced solubility. Using a high-yield *Escherichia coli* expression system, we routinely produced uniformly labeled [^{2}H,^{13}C,^{15}N]CcP samples with high levels of deuterium incorporation (96−99%) and good yields (30−60 mg of pure protein from 1 L of bacterial culture). In addition to simplifying the purification procedure, introduction of a His tag at either protein terminus dramatically increases its solubility, allowing preparation of concentrated, stable CcP samples required for multidimensional NMR spectroscopy. Using a range of biophysical techniques and X-ray crystallography, we demonstrate that the engineered His tags neither perturb the structure of the enzyme nor alter the heme environment or its reactivity toward known ligands. The His-tagged CcP constructs remain catalytically active yet exhibit differences in the interaction with cytochrome *c*, the physiological binding partner, most likely because of steric occlusion of the high-affinity binding site by the C-terminal His tag. We show that protein perdeuteration greatly increases the quality of the double- and triple-resonance NMR spectra, allowing nearly complete backbone resonance assignments and subsequent study of the CcP by heteronuclear NMR spectroscopy.

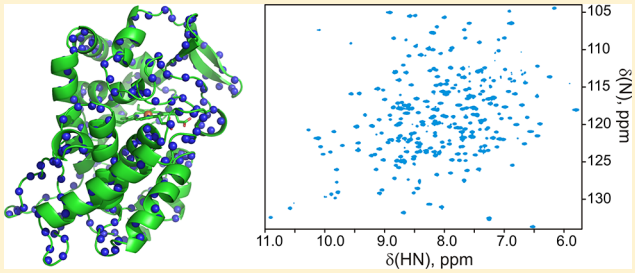

Yeast cytochrome *c* peroxidase (CcP) is a 34.2 kDa heme-containing enzyme that catalyzes reduction of hydroperoxides using the electrons provided by its physiological binding partner cytochrome *c* (Cc). The catalytic mechanism of H_2O_2 reduction involves formation of CcP Compound I (CpdI), an intermediate oxidized 2 equiv above the CcP Fe(III) resting state and containing Fe(IV)═O heme oxyferryl and W191 cation radical.[1] Subsequent CpdI reduction occurs in two one-electron steps, involving complex formation with ferrous Cc, intermolecular electron transfer (ET), and product dissociation. Discovered more than 70 years ago,[2,3] CcP has been widely investigated, and its complex with Cc has become a paradigm for the study of biological ET.[1] However, despite the remarkable attention bestowed on this system, several research questions remain unanswered, including the mechanistic details of the CpdI reduction, the location of the low-affinity Cc binding site active in direct heme-to-heme ET,[4,5] and the relevance of the crystallographic structures of the resting-state CcP−Cc complexes for the description of the reactive Cc−CpdI species in solution.[6]

In principle, the latter two issues can be addressed by high-resolution nuclear magnetic resonance (NMR) spectroscopy, a powerful technique for structural characterization of biomolecular interactions in solution. Until now, the Cc−CcP NMR studies relied on observables reported either by hyperfine-shifted heme resonances of ferric Cc and low-spin, CN-bound CcP, detected in one-dimensional (1D) ^{1}H spectra, or by backbone amide protons of isotopically enriched ^{15}N-labeled Cc, observed in two-dimensional (2D) heteronuclear single-quantum coherence (HSQC) experiments (see ref 6 and references cited therein). The latter detection scheme—employing the uniformly labeled [^{15}N]Cc and the unlabeled, natural abundance CcP—allowed mapping of the Cc surface involved in CcP binding in solution.[7] Recent studies of the Cc−CcP complex by paramagnetic relaxation enhancement (PRE) NMR spectroscopy, observing the intermolecular paramagnetic effects from a spin-label attached to the surface of CcP on the [^{15}N]Cc nuclei, characterized the dominant binding orientation and delineated a transient encounter complex formed on the path of the biomolecular association.[8,9]

However, the Cc-observed experiments alone are insufficient for the full structural characterization of the Cc−CcP

Received: February 20, 2013
Revised: March 16, 2013
Published: March 21, 2013

   dx.doi.org/10.1021/bi400220w | *Biochemistry* 2013, 52, 2165−2175

interaction in solution as exemplified by the incompleteness of the Cc-based encounter-state mapping[9] or the paucity of structural information for the 2:1 complex.[6] Having a fully assigned HSQC spectrum of CcP would allow complementary CcP-detected experiments, yet until now, its study by heteronuclear NMR spectroscopy, a technique requiring concentrated (millimolar range) and stable (several weeks) protein samples, has been hampered by the low solubility and limited thermal stability of the enzyme. Especially at low ionic strengths, CcP is poorly soluble,[10] and the holoprotein spontaneously crystallizes when dialyzed against distilled water, which serves as an additional purification step in many isolation protocols.[11−13] Though useful for the preparation of the enzyme, the poor solubility thwarts biophysical studies that require high protein concentrations, which is further compounded by the low thermal stability of the enzyme, containing a noncovalently bound, *b*-type heme.[1]

Here we show that the introduction of a hexahistidine [$(His)_6$] tag at either CcP terminus enhances enzyme solubility and facilitates its purification, while having virtually no influence on the structure and heme environment. Further, we describe an efficient protocol for the isolation of highly deuterated, uniformly labeled [U-^{2}H,^{13}C,^{15}N]CcP and demonstrate that perdeuteration greatly increases the quality of its multidimensional NMR spectra. Finally, we present nearly complete backbone resonance NMR assignments of the CN-bound [U-^{2}H,^{13}C,^{15}N]CcP constructs, which indicate that the solution structure of this enzyme is the same as in the crystal. The assigned CcP HSQC spectra open a new avenue in the study of the Cc−CcP interaction by NMR spectroscopy, which among other things could provide a complete description of the conformational space sampled in the encounter complex and establish the location of the low-affinity Cc binding site.

MATERIALS AND METHODS

DNA Constructs. The gene encoding *Saccharomyces cerevisiae* CcP, a 294-amino acid enzyme (EC 1.11.1.5), was synthesized by GenScript, with the nucleotide sequence optimized for *Escherichia coli* codon usage. In this work, the native protein contains MKT as the first three N-terminal residues for the enhanced expression in *E. coli*[12] and T53 and D152 as in the original yeast CcP.[1] A number of constructs, featuring C-terminal or N-terminal His tags and/or pelB signal peptide for periplasmic expression (Table 1), were prepared by polymerase chain reaction (PCR), and the products were cloned into the pET24a(+) expression vector between *Nde*I and *Hin*dIII restriction sites (Figure S1 of the Supporting Information). Two N-terminal $(His)_6$ constructs were generated: MH_6KT, with the His tag inserted after the first methionine, and $MKTH_6$, with the His tag placed after the first three residues (Table 1). The plasmid bearing the gene for the wild-type (wt), non-His-tagged CcP was derived from pET24-CcP$(His)_6$ by introducing two stop codons before the C-terminal His tag using whole plasmid synthesis (WHOPS) PCR.[14]

Table 1. CcP Expression Constructs and Yields

construct	His tag, terminus	protein yield[a] rich medium	^{13}C, ^{15}N	^{2}H, ^{13}C, ^{15}N
(MKT) CcP$(His)_6$	C	85 (apo)	72 (apo)	48−54 (apo)
		74 (holo)	62 (holo)	30[b]−45 (holo)
(pelB) CcP$(His)_6$[c]	C	nd[d]	nd[d]	nd[d]
wt (MKT)CcP	none	100 (apo)	nd[d]	70[b] (apo)
		85 (holo)		59[b] (holo)
MH_6KT-CcP	N	80 (apo)	nd[d]	54[b] (apo)
		60 (holo)		40[b] (holo)
$MKTH_6$-CcP	N	nd[d]	nd[d]	nd[d]

[a]Yield of the purified protein in milligrams per liter of culture. [b]Refolding step included. [c]Periplasmic expression. [d]Not determined.

Protein Expression and Purification. For protein expression, a CcP-containing pET24 plasmid was transformed into BL21(DE3) *E. coli* cells. Several precultures (15 mL of LB and 25 μg/mL kanamycin in 50 mL Falcon tubes), inoculated with freshly transformed cells or their 20% (v/v) glycerol stocks stored at −80 °C, were incubated overnight at 37 °C with 180 rpm agitation. For the production of the natural abundance or isotopically enriched CcP, 1 L of rich medium (LB or TB) or 0.5 L of minimal medium (see below), respectively, in 2 L baffled flasks supplemented with 25 mg/L kanamycin was inoculated with 1−5 mL of the precultures and incubated at 37 °C with 180 rpm agitation until the OD_{600} reached 0.6−0.8. At this point, protein expression was induced with 1 mM IPTG, and cultures were incubated for a further 2−3 h at 37 °C with 180 rpm agitation and harvested by centrifugation (5000 rpm for 15 min). The bacterial pellets were resuspended in 20 mM Tris-HCl, 0.5 M NaCl buffer (pH 8.0) and stored at −80 °C.

For the production of the doubly labeled [U-^{13}C,^{15}N]protein, the minimal medium contained M9 salts (6.8 g/L Na_2HPO_4, 3 g/L KH_2PO_4, and 1 g/L NaCl), 2 mM $MgSO_4$, 0.2 mM $CaCl_2$, trace elements (60 mg/L $FeSO_4{\cdot}7H_2O$, 12 mg/L $MnCl_2{\cdot}4H_2O$, 8 mg/L $CoCl_2{\cdot}6H_2O$, 7 mg/L $ZnSO_4{\cdot}7H_2O$, 3 mg/L $CuCl_2{\cdot}2H_2O$, 0.2 mg/L H_3BO_3, and 50 mg/L EDTA), BME vitamin mix (Sigma), and 1 g/L $^{15}NH_4Cl$ and 2 g/L [$^{13}C_6$]glucose as the sole nitrogen and carbon sources, respectively. For the expression of the triply labeled [U-^{2}H,^{13}C,^{15}N]CcP, the minimal medium was prepared in 99.8% D_2O using anhydrous M9 salts, 2 g/L [$^2H_7$,$^{13}C_6$]glucose, and 1 g/L [^{2}H,^{13}C,^{15}N]Celtone base powder (Cambridge Isotope Laboratories). To further decrease the total H_2O content in the deuterated medium, the aqueous solution of trace elements, vitamins, $MgSO_4$, and $CaCl_2$ was lyophilized and redissolved in D_2O prior to use, antibiotic and IPTG solutions were made in D_2O, and care was taken to minimize the exposure to the air moisture.

To purify the His-tagged CcP, the frozen bacterial pellets were thawed, protease inhibitors added (0.1 mg/mL AEBSF-HCl and 1 μg/mL leupeptin), and cells lysed in a French press (Thermo Scientific) or EmulsiFlex-C5 homogenizer (Avestin). The lysate was cleared by centrifugation (10000 rpm for 30 min), the imidazole added to the final concentration of 5 mM, and the solution loaded at a rate of 2−3 mL/min onto a 5 mL prepacked HisTrap column (GE Healthcare) equilibrated in 20 mM Tris-HCl, 0.5 M NaCl, and 5 mM imidazole (pH 8.0). Once loaded, the column was washed with 10−15 mL of the equilibration buffer, and the protein eluted at a rate of 2−3 mL/min with a 60−120 mL linear gradient from 5 to 500 mM imidazole in 20 mM Tris-HCl and 0.5 M NaCl (pH 8.0). As a rule, the chromatogram recorded at 280 nm shows two major peaks, with the second, more intense one containing CcP (Figure 1). The elution fractions were analyzed by sodium dodecyl sulfate−polyacrylamide gel electrophoresis (SDS−PAGE), and those containing CcP were collected and

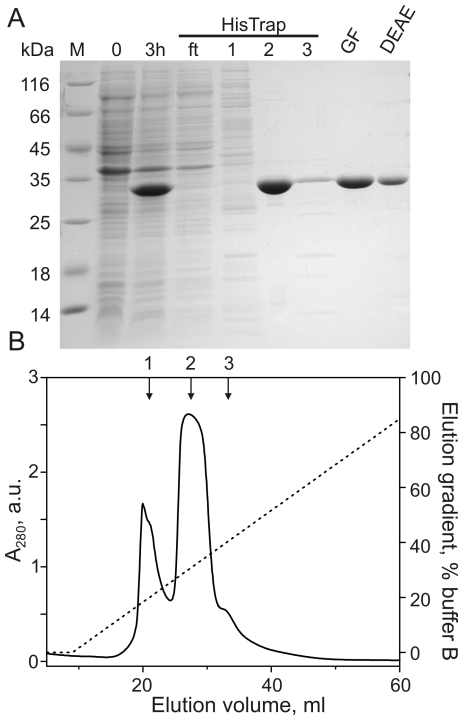

Figure 1. Expression and purification of [U-^{2}H,^{13}C,^{15}N]CcP(His)$_6$. (A) SDS–PAGE. M denotes the molecular weight markers. Lanes labeled with "0" and "3h" refer to the whole-cell extracts of *E. coli* cultures before induction and at harvest, respectively. The remaining lanes show protein samples after purification by immobilized metal affinity chromatography (HisTrap; "ft" is a flow-through, and numbers refer to the protein fractions indicated in panel B), followed by size-exclusion (GF) and ion-exchange (DEAE) chromatography. (B) Chromatogram (—) and elution gradient (···) for the first CcP purification step on a HisTrap column. Arrows indicate protein fractions analyzed by SDS–PAGE in panel A.

concentrated in an Amicon centrifugal device (10000 cutoff; Millipore). The protein was further purified on a Superdex 75 16/90 column (GE Healthcare) equilibrated in 20 mM sodium phosphate (NaP_i) and 100 mM NaCl (pH 6.0) and run at a rate of 1.5 mL/min. The fractions containing pure apo CcP, corresponding to the major chromatogram peak, were pooled, and the protein concentration was estimated spectrophotometrically (ε_{280} = 59.36 mM^{-1} cm^{-1}). For the refolding step (see Results and Discussion), the protein solution was adjusted to 1–1.2 M Gnd-HCl with a buffered 6 M Gnd-HCl stock, incubated for 30–40 min at ambient temperature, and exchanged into 20 mM NaP_i and 100 mM NaCl (pH 6.0) on a HiPrep 26/10 desalting column (GE Healthcare) run at a rate of 10 mL/min.

For cofactor insertion, apo CcP was dialyzed against 100 mM NaP_i and 5 mM sodium ascorbate (pH 7.5) (6000 cutoff dialysis membranes; Spectra-Por) at 4 °C, combined with the hemin solution, and dialyzed further against 20 mM NaP_i and 5 mM sodium ascorbate (pH 6.0) at 4 °C. The hemin solution was prepared gravimetrically by dissolving a slight excess (typically 1.2–1.3 equiv) of porcine hemin (Sigma) in 0.5–1 mL of 0.1 M NaOH and subsequently diluting it into ~40 mL of dialysis buffer. All hemin manipulations were performed in the dark to minimize its photodegradation. After the overnight dialysis, the protein solution was loaded onto a DEAE column (GE Healthcare) equilibrated in 20 mM NaP_i (pH 6.0) and eluted at a rate of 3 mL/min with a 360 mL linear gradient from 0 to 0.5 M NaCl in the same buffer. The reconstituted holo CcP eluted in a single peak, leaving a dark-brown band of the excess free hemin irreversibly bound to the top layer of the column material (discarded after use). The holo CcP was exchanged into 20 mM NaP_i and 100 mM NaCl (pH 6.0), and its concentration and purity were estimated from the electronic absorption (UV–vis) spectra using an ε_{410} of 105 mM^{-1} cm^{-1} (see below) and an A_{410}/A_{280} of >1.2,[13,15] respectively. Typical yields for different protein preparations are listed in Table 1.

The native, non-His-tagged protein was purified in an analogous fashion, except for the first chromatographic step [ion-exchange Source 30Q column (GE Healthcare), elution at a rate of 5 mL/min with a 500 mL linear gradient from 0 to 1 M NaCl in 20 mM Tris-HCl (pH 8.0)] and the final crystallization of the reconstituted holo CcP by dialysis against deionized water as described elsewhere.[12] Recombinant equine cytochrome *c* (hCc) and yeast iso-1-cytochrome *c* (yCc) were prepared as described previously.[16]

Mass Spectrometry. The samples were prepared by desalting the purified proteins on a C18 SPE column (Thermo Scientific) and then diluted with the 50:50 (v/v) acetonitrile/water mixture containing 0.1% formic acid to an approximate concentration of 5 μM. The protein solutions were introduced by an off-line infusion using a capillary electrospray at a rate of 1.5 μL/min. An LTQ XL mass spectrometer (Thermo Fisher Scientific) was used to acquire mass spectra from m/z 400 to 2000 in centroid mode. Electrospray source conditions such as "source fragmentation" voltage and the tube lens voltage were optimized to help desolvation, but without fragmenting the intact protein. Default values were used for most of the other data acquisition parameters. The resulting spectra were averaged up to 200 scans and deconvoluted with ProMass (Thermo Fisher Scientific).

Electronic Absorption and Circular Dichroism Spectroscopy. The electronic absorption spectra were recorded on a Cary 100 Bio (Varian) spectrophotometer at 22 °C in 20 mM NaP_i (pH 6.0). Continuous scans in the 250–750 nm region were taken using a 1 cm cuvette, a scan rate of 600 nm/min, a bandwidth of 2.0 nm, and a resolution of 1 nm. For the CcP–ligand complexes with a 1:1 stoichiometry, K_D = ([CcP][L])/[CcP–L] and [CcP]/[CcP–L] = (ΔA_0 − ΔA)/ΔA,[17] where [CcP], [L], and [CcP–L] are equilibrium concentrations of the free enzyme, free ligand, and enzyme–ligand complex, respectively; ΔA_0 is the difference in absorption between the fully bound and free enzyme, and ΔA is the absorption change at each titration point. Combining the two equations yields eq 1:

$$\Delta A = \Delta A_0[L]/(K_D + [L]) \quad (1)$$

which was used to fit the titration curves, with ΔA_0 and K_D as the free parameters.

CD spectra were recorded on a J-715 spectropolarimeter (Jasco) at room temperature in 20 mM NaP_i and 100 mM NaCl (pH 6.0) with a CcP concentration of 0.5 mg/mL. Continuous scans were taken using a 1 mm cuvette, a scan rate of 50 nm/min, a bandwidth of 1.0 nm, and a resolution of 0.5 nm, with the CD spectra averaged over six consecutive scans. The raw CD data (ellipticity θ in millidegrees) were normalized for protein concentration and the number of residues, yielding the mean residue ellipticity ([θ] in degrees square centimeters per mole): [θ] = $\theta M_r/(nCl)$, where M_r, n, C, and l are the molecular mass (in daltons), the number of CcP residues, the

dx.doi.org/10.1021/bi400220w | *Biochemistry* 2013, 52, 2165–2175

protein concentration (in milligrams per milliliter), and the cuvette path length (in centimeters), respectively.

X-ray Crystallography. The initial crystallization screen was performed with six commercial crystallization kits (HR-Index, HR-Crystal Screen I & II, MD-Proplex, MD-PACT, Qiagen JCSG+) using the sitting drop method. In a Phoenix crystallization robot (Art Robbins Instruments), 100 nL of the 5, 10, and 15 mg/mL solutions of the CcP complex with the fluoride [CcP(His)$_6$-F] was mixed with 100 nL of the reservoir solution in three-well Intelliplates (Art Robbins Instruments), and the reservoir was filled with 80 μL of the precipitant solution to equilibrate the drops. Condition A8 from the PACT premier screen [catalog no. MD1-36; crystallization conditions, 0.2 M NH_4Cl, 0.1 M CH_3COONa (pH 5.0), and 20% (w/v) PEG 6000] produced crystals after 5 days at 20 °C for protein concentrations of 10 and 15 mg/mL. The crystallization was optimized by the hanging drop method in a 24-well plate (Hampton Research), where the PEG 6000 concentration was varied from 14 to 24% in 2% steps, while buffer and salt concentrations were kept constant. A complete X-ray diffraction data set was collected from a single CcP(His)$_6$-F crystal, cryocooled in liquid nitrogen using the reservoir solution supplemented with 20% glycerol as a cryoprotectant.

The X-ray diffraction data (180 images acquired with an oscillation step of 1° and a 5 min exposure time) were collected in house on a MicroMAx-007 HF source generator (Rigaku). The diffraction intensities were integrated, merged, and scaled with the HKL 3000 suite.[18] The structure was determined by molecular replacement using HKL 3000,[18] with the coordinates of the resting-state CcP [Protein Data Bank (PDB) entry 1ZBY][19] as the search model. Manual building and placement of water molecules and the heme were performed using COOT.[20] The structure was refined by Refmac5,[21] and stereochemical validations were made with PROCHECK.[22] Coordinates and structure factors have been deposited in the Protein Data Bank as entry 4JB4. See Table S1 of the Supporting Information for the data collection and refinement statistics.

NMR Spectroscopy. Backbone assignment experiments were conducted at 298 K on a four-channel Varian NMR Direct-Drive 800 MHz spectrometer equipped with a salt-tolerant PFG-Z cold probe. The samples contained 1−1.5 mM [^{2}H,^{13}C,^{15}N]CcP(His)$_6$-CN or MH$_6$KT CcP-CN in 20 mM NaP_i, 100 mM NaCl (pH 6.0), and 6% D_2O for the lock. The assignments were obtained from a series of TROSY-selected 2D ^{1}H−^{15}N HSQC, three-dimensional (3D) HNCO, and deuterium-decoupled 3D HN(CA)CO, HNCA, HN(CO)CA, and out-and-back HN(CA)CB spectra. All NMR data were processed in NMRPipe[23] and analyzed in CCPN.[24] The resonance assignments determined in this work were deposited in the BioMagResBank as entries 19004 and 19005.

For the Cc-observed NMR titrations, 1D ^{1}H spectra (with water presaturation) were acquired on a Varian NMR Direct-Drive 600 MHz spectrometer. The titration experiments were performed by an incremental addition of a concentrated stock solution of ferric yCc to a 0.3 mM solution of CcP (both at natural abundance) at 303 K in 20 mM NaP_i, 100 mM NaCl (pH 6.0), and 6% D_2O. The NMR chemical shift titration curves were analyzed with a two-parameter nonlinear least-squares fit using a one-site binding model corrected for the dilution effect (eq 2):[25]

$$\Delta\delta_{\text{binding}} = 0.5\Delta\delta_0\left(A - \sqrt{A^2 - 4/R}\right)$$

$$A = 1 + 1/R + \frac{[\text{Cc}]_0 + R[\text{CcP}]_0}{R[\text{Cc}]_0[\text{CcP}]_0 K_B} \quad (2)$$

where $\Delta\delta_{\text{binding}}$ is the chemical shift perturbation at a given protein ratio, $\Delta\delta_0$ is the chemical shift perturbation at 100% Cc bound, R is the [Cc]/[CcP] ratio at a given point, $[\text{Cc}]_0$ and $[\text{CcP}]_0$ are the concentrations of the protein stock solution used for the titration and the starting solution, respectively, and K_B is the binding constant. Thus, $\Delta\delta_{\text{binding}}$ and R are the dependent and independent variables, respectively, and $\Delta\delta_0$ and K_B are the fitted parameters.

Steady-State Kinetics. Following an established protocol,[26,27] oxidation of horse ferrocytochrome *c* (hCc) was monitored at 550 nm on Cary 100 Bio (Varian) spectrophotometer. A stock of the ferrous hCc was prepared by reduction of the oxidized protein with an excess of sodium ascorbate and subsequent protein elution from a desalting PD10 column (GE Helthcare). All experiments were performed in 20 mM NaP_i and 100 mM NaCl (pH 6.0) at 22 °C. The concentrations of CcP and H_2O_2 were held constant, while that of hCc was varied in the range of 2−100 μM. The reaction was initiated by addition of H_2O_2. Initial velocities (v_o) were determined from the initial slopes of the kinetic traces as $v_0 = \Delta A/(2\Delta\varepsilon_{550}\Delta t)$, where $\Delta A/\Delta t$ is the change in absorption versus time, $\Delta\varepsilon_{550}$ (19.5 mM^{-1} cm^{-1}) is the difference in the absorptivity of ferro- and ferricytochrome, and the factor 2 accounts for two molecules of hCc reduced per catalytic cycle.[26,27] As described in the literature,[26,27] the initial velocities were corrected for the uncatalyzed reaction of ferrocytochrome *c* with H_2O_2 (typically 10−15% of the CcP-catalyzed rate) and the inhibition by the oxidized hCc (present up to 5% in the protein stock). The data were analyzed by a nonlinear fit to several kinetic models[28] (eq 3), with model selection performed using F statistics as described in Results and Discussion.

$$\frac{v_0}{e} = \frac{V_1/e[\text{Cc}]}{K_{M1} + [\text{Cc}]} + \begin{cases} 0, & \text{model 1} \\ \dfrac{V_2/e}{K_{M2}}[\text{Cc}], & \text{model 2} \\ \dfrac{V_2/e[\text{Cc}]}{K_{M2} + [\text{Cc}]}, & \text{model 3} \end{cases} \quad (3)$$

where [Cc] is the ferrocytochrome *c* concentration, V_1/e and V_2/e are the maximal turnover numbers for the two kinetic phases, and K_{M1} and K_{M2} are the corresponding Michaelis constants.

RESULTS AND DISCUSSION

Expression and Purification. To determine the optimal overexpression conditions for His-tagged CcP constructs, CcP(His)$_6$ was produced in the cytoplasm or periplasm of BL21(DE3) *E. coli* at two different temperatures in Luria-Bertani (LB), Terrific Broth (TB), and Super Broth (SB) media. As can be seen from Figure S2 of the Supporting Information, high CcP expression levels were obtained throughout, with the optimal conditions being postinduction growth for 2−4 h in LB or TB at 30 °C for the periplasmic and either 30 or 37 °C for the cytoplasmic constructs. For the latter, most of the CcP was recovered in the soluble fraction upon lysis (Figure S3A of the Supporting Information), and a

similarly high expression level was observed in ^{13}C- and ^{15}N-labeled minimal medium (MM) (Figure S3B of the Supporting Information). Thus, the cytoplasmic expression at 37 °C was chosen for all subsequent protein preparations.

An analogous protocol was used for expression of the perdeuterated CcP. To ensure high levels of deuterium incorporation, we used MM in 99.8% D_2O and [$^2H_7$,$^{13}C_6$]-glucose as the sole carbon source. Further, to stimulate bacterial growth in D_2O medium, the cultures were spiked with [^2H,^{13}C,^{15}N]Celtone, resulting in an ~1 h bacterial doubling time. Contrary to an earlier report,[15] no adaptation of *E. coli* to D_2O was found to be necessary; cultures started from either freshly transformed BL21(DE3) cells or their aqueous glycerol stocks exhibited healthy growth and high expression levels under the conditions used.

One-step purification of CcP(His)$_6$ by immobilized metal affinity chromatography (IMAC) yields an essentially pure protein (Figure 1). During an additional size-exclusion chromatography step, CcP elutes as a single peak, well separated from a minor band of high-molecular weight impurities. The yields of different apo CcP preparations, estimated at this point, are listed in Table 1. After insertion of the heme into the apo protein, the holo CcP is purified by ion-exchange chromatography, with final yields varying from 30 to 85 mg/L of culture, depending on the construct and the isotope labeling scheme (Table 1). The yields of natural abundance proteins obtained in this work are comparable to those for the original CcP(MKT) *E. coli* expression system[12] and are 3−5 times higher than those reported for the recombinant CcP with the native sequence.[13,15] For the perdeuterated CcP, we achieved a 3−5-fold increase in the protein yields and higher levels of deuterium incorporation (see below) compared to those of an earlier work.[15] The introduced His tag greatly simplifies the CcP purification procedure, affording a 2-fold decrease in the total preparation time compared to that of the original method.[12] Using the protocol given in Materials and Methods, we routinely produced highly pure, reconstituted holo proteins in 3−4 days.

In addition to CcP(His)$_6$, we also prepared two N-terminally His-tagged constructs, MH$_6$KT and MKTH$_6$, with the His tag inserted after the first methionine and after the first three residues, respectively. It was shown that the CcP featuring MKT at the N-terminus gives high expression levels in *E. coli*,[12] which is confirmed in this work for the wt and CcP(His)$_6$ proteins, both starting with the MKT. Thus, we reasoned that the MKTH$_6$ construct could be produced in higher yields. However, contrary to our expectations, the expression level of the MKTH$_6$ CcP turned out to be somewhat smaller than that of the MH$_6$KT CcP, and overall, the N-terminally His-tagged constructs expressed less well than the C-terminally His-tagged protein (Figure S4 of the Supporting Information). Consequently, here we present extensive characterization of CcP(His)$_6$, our His-tagged construct with the highest expression level, and, to a lesser extent, MH$_6$KT CcP and compare their properties to those of the wt enzyme.

Protein Solubility and Long-Term Storage. Unlike the non-His-tagged protein, which readily crystallizes upon dialysis against H_2O at 4 °C, the holo CcP(His)$_6$ remains soluble under these conditions at concentrations exceeding 0.1 mM. With the solubility of the wt CcP estimated to be <10 μM at zero ionic strength and 4 °C,[10] it appears that the His tag renders the protein at least 10 times more soluble. In line with these findings, as confirmed by dynamic light scattering (DLS) and electronic absorption spectrophotometry (UV−vis), 0.3 mM samples of the CN-bound CcP, CcP(His)$_6$-CN, remained stable in 20 mM NaP$_i$ or MES (pH 6.0) at 25 °C for at least 48 h (analysis not conducted for longer periods of time). Further, in contrast to our previous experience in which 0.7 mM samples of the wt CcP would aggregate overnight at 25 °C (A. N. Volkov, unpublished observations), solutions containing 1−1.5 mM [U-^2H,^{13}C,^{15}N]CcP(His)$_6$-CN or MH$_6$KT CcP-CN in 20 mM NaP$_i$ and 100 mM NaCl (pH 6.0) were stable for at least 12−14 days at 25 °C (see below). Thus, introduction of a His tag allows the preparation of concentrated, stable protein samples suitable for multidimensional NMR experiments.

To identify the optimal long-term storage conditions, solutions of the resting-state CcP(His)$_6$ in H_2O were lyophilized or frozen at −20 and −80 °C. Circular dichroism (CD), DLS, and UV−vis experiments were performed before and after the storage to determine its effect on the CcP secondary structure, aggregation status, and heme coordination properties, respectively. While the CD and DLS for both lyophilized and frozen samples remained virtually identical, the UV−vis spectrum of the former exhibited a 3 nm blue shift of the Soret band and a >5% decrease in the A_{Soret}/A_{280} ratio, indicating changes in the heme coordination environment. At the same time, the UV−vis spectrum of the protein stored for more than 40 days at −80 °C remained unchanged. Thus, lyophilization was avoided and the purified resting-state CcP routinely stored in either H_2O or 20 mM NaP$_i$ and 100 mM NaCl (pH 6.0) at −20 or −80 °C.

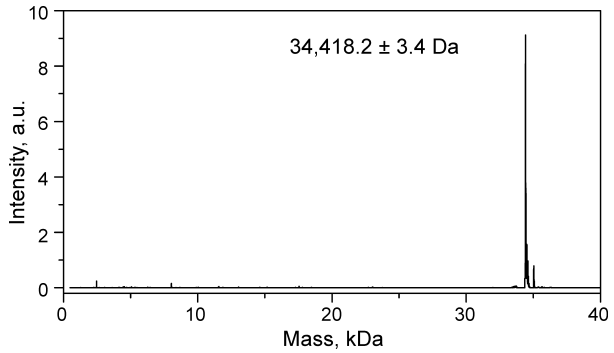

Figure 2. Deconvoluted ESI-MS spectrum of the natural abundance CcP(His)$_6$. The main peak, with the indicated mass, corresponds to the 300-amino acid polypeptide (Table 2).

Mass Spectrometry. The purified CcP(His)$_6$ was characterized by electrospray ionization mass spectrometry (ESI-MS). The mass spectrum is dominated by a single peak,

Table 2. ESI-MS Analysis of Different CcP(His)$_6$ Preparations

labeling	mass (Da)[a]
na[b]	34418.2 ± 3.4 (34416.3)
^{13}C, ^{15}N	36349.4 ± 3.8 (36382.3)
^2H, ^{13}C, ^{15}N	38152 ± 3.7[c] (38692.3)[d]
	37000 ± 3.2[e] (38140.3)[f]

[a]Theoretical values are given in parentheses. [b]Natural isotope abundance. [c]CcP preparation without the refolding step. [d]Calculated for 100% deuterated protein. [e]CcP preparation with the refolding step. [f]Calculated for the protein deuterated only at nonlabile hydrogen positions.

dx.doi.org/10.1021/bi400220w | *Biochemistry* 2013, 52, 2165−2175

corresponding to the His-tagged CcP polypeptide retaining the N-terminal methionine (Figure 2). The intact masses of the proteins produced with different labeling schemes are listed in Table 2. Comparison of the experimentally determined and theoretical molecular weights of the isotopically enriched CcP was used to estimate the extent of isotope incorporation, which was found to be 99.9% for [U-^{13}C,^{15}N]CcP(His)$_6$ and 95.6–98.6% for [U-^{2}H,^{13}C,^{15}N]CcP(His)$_6$. Thus, it appears that supplementing the D_2O medium with [^{2}H$_7$,^{13}C$_6$]glucose and [^{2}H,^{13}C,^{15}N]Celtone yields high levels of protein deuteration, up from the value of 84% reported previously.[15]

Electronic Absorption and Circular Dichroism Spectroscopy. The UV–vis spectrum of the resting-state CcP(His)$_6$ features a number of absorption bands characteristic of a five-coordinate heme group (Figure 3A) and is highly similar to

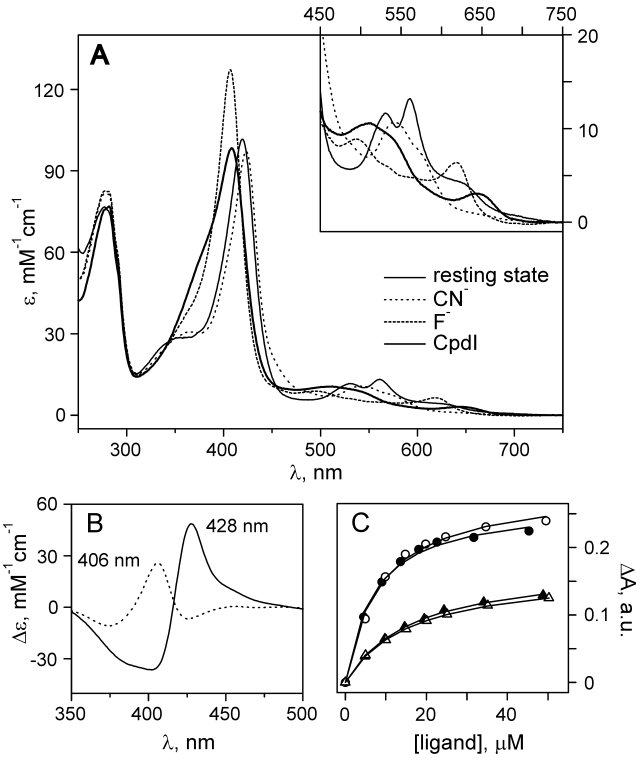

Figure 3. Electronic absorption spectroscopy of holo CcP(His)$_6$. (A) Absorption spectra of the enzyme in different ligation and spin states in 20 mM NaP$_i$ (pH 6.0) at 22 °C. Absorption maxima and the corresponding extinction coefficients are listed in Table 3. The inset shows expansion of the 450–750 nm region. (B) Difference spectra between CN^--bound (—) and F^--bound (---) forms and the resting-state enzyme. The absorption maxima are indicated. (C) Titration curves for the binding of CN^- (circles) and F^- (triangles) to 4.53–5.02 μM CcP(His)$_6$ in the absence (filled symbols) and presence (empty symbols) of 100 mM NaCl. The solid lines show the fit of the data to eq 1 (Materials and Methods). The K_D values are listed in Table 3.

that of the native, wt enzyme.[29] Just as the wt protein, the CcP(His)$_6$ binds F^- and CN^- ions, giving rise to electronic absorption spectra typical for the six-coordinate heme with a low- or high-spin Fe(III) atom (F- or CN-bound form, respectively).[30] Binding of these ligands can be followed in the UV–vis difference spectra (Figure 3B,C), which was used to extract the corresponding equilibrium dissociation constants (K_D). The K_D values obtained in this work (Table 3) are in

Table 3. Spectral Parameters and Binding Constants for the CcP(His)$_6$–Ligand Complexes in 20 mM NaP$_i$ (pH 6.0) at 22 °C[a]

CcP form	λ_{max}[b] (nm)	$\varepsilon(\lambda_{max})$[c] ($mM^{-1}$ cm^{-1})	K_D (μM)[d]
resting state	408 (410)	98.0[e] (105.1)	
CN^-	423 (423)	97.3 (98.0)	7.1 ± 0.6 (8.6 ± 0.9)
F^-	407 (407)	127.2 (129.0)	16.5 ± 0.7 (16.2 ± 0.3)
CpdI	419 (419)	101.7 (99.7)	

[a]The values in parentheses are for the samples containing 100 mM NaCl. See Figure 3 for details. [b]Absorption maximum. [c]Extinction coefficient at the absorption maximum. [d]Equilibrium dissociation constant for CN^- and F^- binding (Figure 3C). [e]Value taken from ref 43 and used to calculate all other $\varepsilon(\lambda_{max})$ values reported in this work.

agreement with the previously reported K_D values of 2–6 μM[17,31] and 16–30 μM[32,33] for the CcP-CN and CcP-F complexes, respectively. Interaction of the CcP(His)$_6$ with H_2O_2 leads to the formation of the CcP CpdI with a characteristic UV–vis spectrum dominated by the absorption of the Fe(IV)=O heme oxyferryl.[29] The absorption maxima and the corresponding extinction coefficients for different CcP(His)$_6$ forms are listed in Table 3. The UV–vis spectra of MH$_6$KT CcP (Figure S5 of the Supporting Information) are virtually identical to those of CcP(His)$_6$, and the spectra of both His-tagged constructs are highly similar to those of the native, wt enzyme,[29] suggesting that introduction of the His tag at either terminus does not perturb the heme environment.

The far-UV CD spectra of the resting-state and CN-bound CcP(His)$_6$ show that the protein adopts a globular structure with a high α-helical content (Figure S6 of the Supporting Information). The high level of similarity of the CD spectra to those of the wt CcP[34] indicates that the presence of a His tag does not affect the overall fold of the protein.

X-ray Crystallography. To complete the structural characterization of the His-tagged protein, we performed crystallographic analysis of the CcP(His)$_6$ in the F-bound form. At the backbone level, the CcP(His)$_6$-F structure (refined to 2.42 Å resolution) is very similar to that of the resting-state wt enzyme, with a root-mean-square deviation (rmsd) of 0.29 Å for the C$_\alpha$ atoms (Figure 4). Compared to the high-resolution

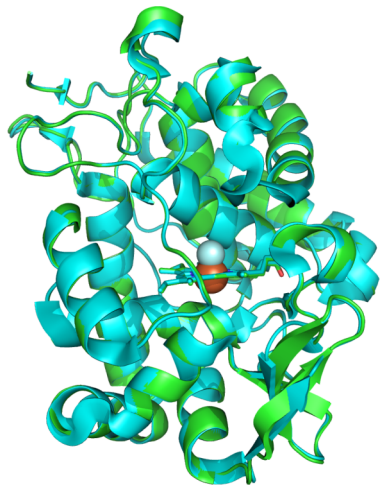

Figure 4. Overlay of the X-ray structures of the CcP(His)$_6$-F (this work, green) and the resting-state CcP (PDB entry 1ZBY,[17] cyan). Heme groups are shown as sticks and Fe and F atoms as spheres.

dx.doi.org/10.1021/bi400220w | Biochemistry 2013, 52, 2165–2175

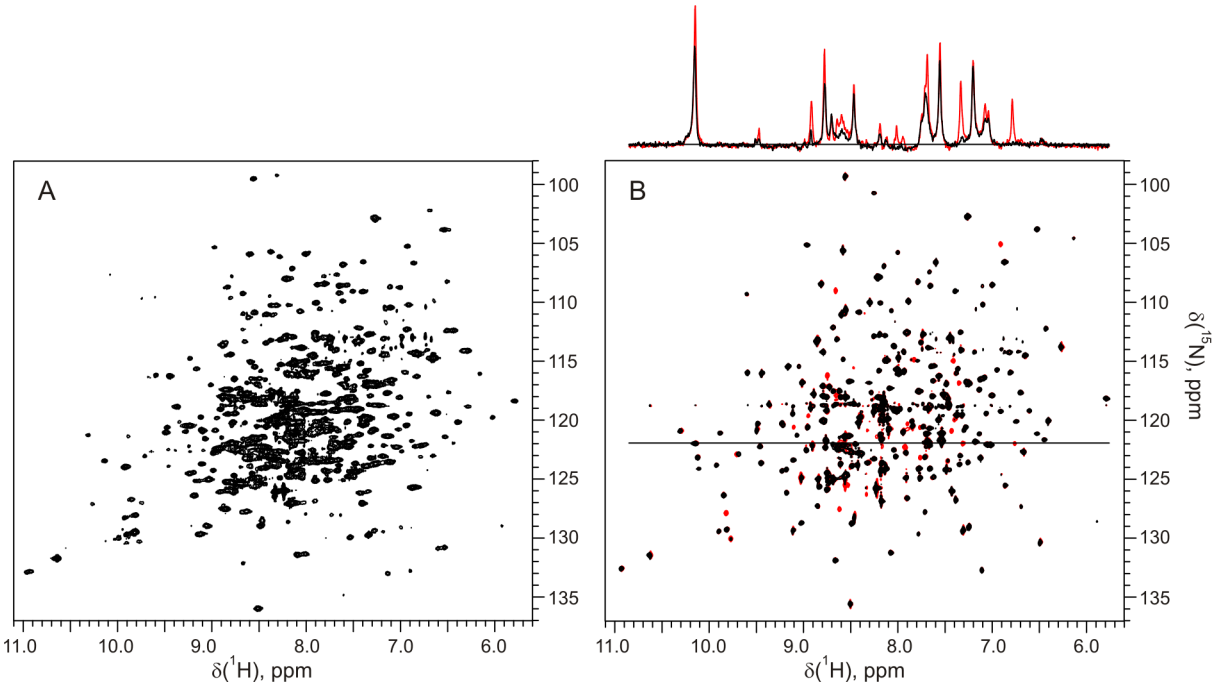

Figure 5. NMR spectra of the protonated and perdeuterated CcP. Two-dimensional $^{1}H-^{15}N$ TROSY-HSQC spectra of (A) 1 mM [U-^{13}C,^{15}N]CcP(His)$_6$-CN and (B) 1.2 mM [U-^{2}H,^{13}C,^{15}N]CcP(His)$_6$-CN in 20 mM NaP_i and 100 mM NaCl (pH 6.0) at 298 K, acquired with the same spectral widths and number of increments (16.1 ppm and 2048 points in the ^{1}H dimension and 44 ppm and 128 points in the ^{15}N dimension) but with a different number of scans: 16 in panel A and 8 in panel B. Note that the contour levels in panels A and B differ. (B) Spectra of the CcP samples prepared with and without the refolding step are colored red and black, respectively. The 1D traces show slices taken through the spectra at the position indicated by the solid line.

structure of the resting-state CcP (PDB entry 1ZBY),[19] which features two side-chain conformations for residues R48 and M172 and alternative backbone and side-chain orientations for residues A193, A194, and N195, the six-coordinate, CcP(His)$_6$-F form appears to be more ordered. In agreement with the X-ray structures of the wt CcP-F (for which no coordinates are available in the PDB),[35,36] residue R48 is in the "in" conformation, M172 in the orientation closer to the heme iron ligand H175, and the region of A193−N195 described well by a single conformation. As seen in the F-bound and CpdI forms of the wt enzyme, these structural changes are believed to accommodate the heme iron ligand and contribute to stabilization of the H-bond network involving proximal H175.[19,35,36] In line with the biophysical and spectroscopic evidence presented above, the crystallographic analysis of CcP(His)$_6$-F confirms that introduction of a His tag does not perturb the protein structure or alter its heme environment.

NMR Spectroscopy. In this work, the NMR experiments were performed on the low-spin, CN-bound CcP form, whose NMR spectra suffer less from the paramagnetic line broadening induced by the heme iron than those of the high-spin, resting-state enzyme.[37,38] The $^{1}H-^{15}N$ TROSY-HSQC spectrum of the [^{13}C,^{15}N]CcP(His)$_6$-CN shows good peak dispersion characteristic of a well-folded, globular protein (Figure 5A). However, because of the fast transverse relaxation expected for a 36 kDa enzyme, most of the resonances are very broad, which greatly decreases the resolution in both ^{1}H and ^{15}N dimensions. Moreover, the similarly low resolution of the triple-resonance spectra of the ^{13}C- and ^{15}N-labeled sample (Figure S7 of the Supporting Information) makes backbone amide assignments a daunting task. To improve the NMR properties of CcP, we prepared a perdeuterated enzyme, in which most nonlabile protons are substituted with ^{2}H atoms. Often used for the NMR study of high-molecular weight proteins, deuteration is known to decrease the backbone amide transverse relaxation rate, leading to an increased signal-to-noise ratio and improved resolution.[39] Indeed, the double- and triple-resonance spectra of [^{2}H,^{13}C,^{15}N]CcP(His)$_6$-CN (Figure 5 and Figure S7 of the Supporting Information) feature sharp, well-resolved peaks and are of sufficient quality for the resonance assignment.

At the initial assignment stage, we could not detect resonances for the two continuous stretches of residues 19−45 and 95−133. As many of these groups, especially in the second stretch, are buried inside the protein, we surmised that an incomplete exchange of the initial, NMR-silent backbone amide deuterons for the NMR-visible protons was to blame. To facilitate the amide exchange at buried sites, the apo [^{2}H,^{13}C,^{15}N]CcP(His)$_6$ was partially unfolded in 1−1.2 M GndHCl, incubated at room temperature to allow deuterium-to-proton substitution, and refolded into the denaturant-free buffer. The refolded apo protein was purified further as usual (see Materials and Methods). Overall, the resonances common to the spectra of both refolded and untreated [^{2}H,^{13}C,^{15}N]-CcP(His)$_6$-CN remain the same (e.g., compare the black and red traces in Figure 5B), indicating that the refolding does not perturb the structure of the protein. In addition to the resonances observed previously, the $^{1}H-^{15}N$ TROSY-HSQC spectrum of the refolded [^{2}H,^{13}C,^{15}N]CcP(His)$_6$-CN features extra peaks (compare the black and red spectra in Figure 5B), which indeed originate from residues 19−45 and 95−133 (Figure S8 of the Supporting Information). Comparison of the $^{1}H-^{15}N$ TROSY-HSQC spectra recorded before and after the acquisition of triple-resonance NMR assignment experiments shows that the [^{2}H,^{13}C,^{15}N]CcP(His)$_6$-CN sample remains

dx.doi.org/10.1021/bi400220w | *Biochemistry* 2013, 52, 2165−2175

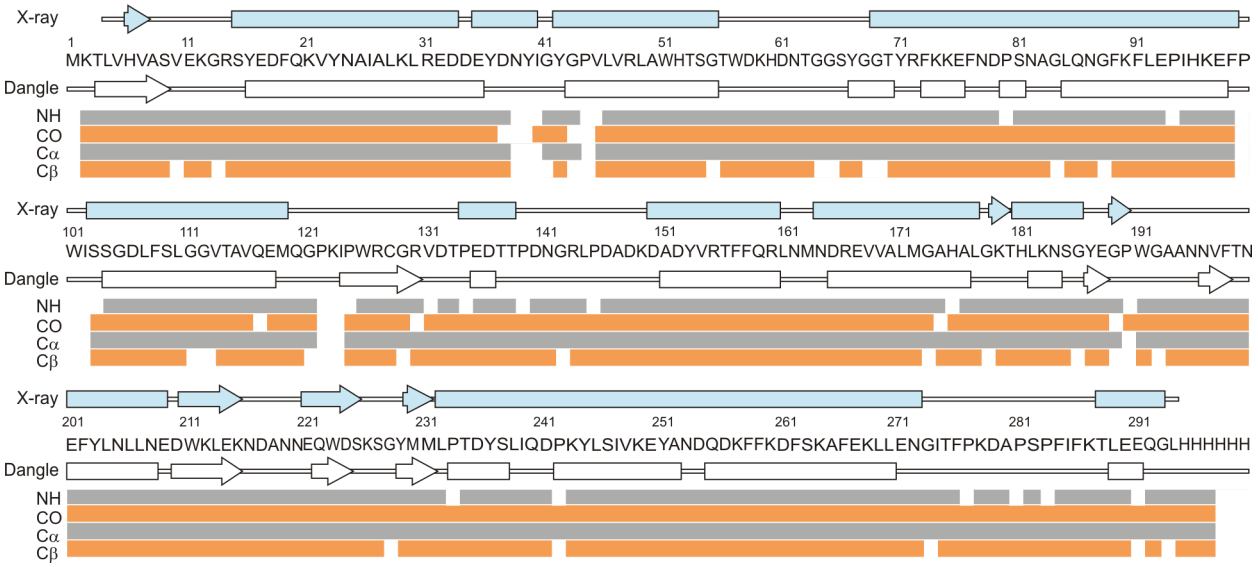

Figure 6. Extent of the NMR resonance assignments and secondary structure of [U-^{2}H,^{13}C,^{15}N]CcP(His)$_6$-CN. Assigned resonances of the protein backbone atoms are indicated by colored bars. Secondary structure (bars, α-helices; arrows, β-sheets) predicted with DANGLE[44] from the backbone chemical shifts (white) is compared to that observed in a high-resolution X-ray structure (blue, PDB entry 1ZBY).[19]

stable for the entire duration of the measurements (12−14 days).

Using the refolded [^{2}H,^{13}C,^{15}N]CcP(His)$_6$-CN protein, we obtained nearly complete assignments of the N, HN, C_α, C_β, and CO nuclei (Figure 6). No assignments could be derived for any atom of residues M1, N38, Y39, P44, P100−I102, P122−I124, and H298−H300. In addition, the following resonances could not be assigned: I40 and P190 (C_α); V10, I40, P190, P242, and E291 (C_β); D37, G43, Q117, R130, A174, and G189 (CO); and I40, V45, S103, V131, H175, and E291 (NH). In total, the unambiguous assignments were obtained for 94.7% NH, 93.7% CO, 95.0% C_α, and 93.5% C_β atoms. Thus, of 285 non-proline residues present in the protein, backbone amides of 269 could be unambiguously assigned in the 2D ^{1}H−^{15}N TROSY-HSQC spectrum (Figure 5 and Figure S8 of the Supporting Information). The unambiguous assignments of [^{2}H,^{13}C,^{15}N]MH$_6$KT CcP-CN were obtained for 91.9% NH, 87.0% CO, 93.3% C_α, and 92.0% C_β atoms, with seven more unassigned NH resonances (V10, Y23, I26, D34, E35, R130, and L294) and two new NH assignments (N38 and Y39) compared to those of the C-terminally His-tagged protein (Figures S9 and S10 of the Supporting Information). Except for the residues in the proximity of the protein termini, the backbone amide chemical shifts of the two CcP constructs are very similar (Figure S11 of the Supporting Information). This finding confirms that the introduction of the His tag at either terminus does not perturb the protein structure, as already shown by the crystallographic analysis (see above). For both CcP constructs, the secondary structure prediction from the backbone chemical shifts is in excellent agreement with the X-ray structure (Figure 6 and S9 of the Supporting Information), suggesting that the crystallographic and solution structures of the enzyme are the same.

Steady-State Kinetics. To assess the catalytic activity of the CcP constructs described in this work, we performed steady-state kinetics experiments. Following an established protocol,[26,27] the enzyme and H_2O_2 concentrations were held constant (a large excess of the latter was used throughout to ensure that the reaction is independent of H_2O_2), and oxidation of ferrous horse Cc (hCc) at varying concentrations was followed spectrophotometrically (see Materials and Methods). Under these pseudo-first-order conditions, Cc appears as a substrate; thus, the kinetic parameters characterize Cc oxidation by CcP CpdI rather than H_2O_2 reduction by CcP. As can be seen from Figure 7, all three CcP constructs are catalytically

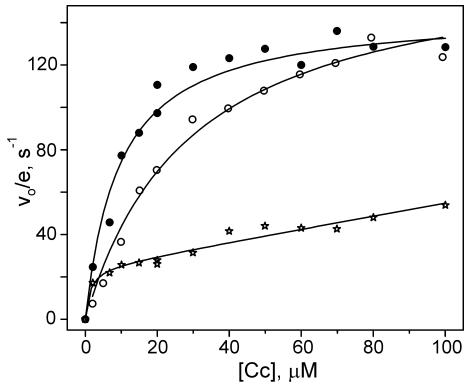

Figure 7. Steady-state kinetics of H_2O_2 reduction by CcP. Pseudo-first-order reduction of CpdI by ferrous hCc, monitored spectrophotometrically (see Materials and Methods), with a constant CcP concentration of 0.88−0.98 nM and 200 μM H_2O_2 at different hCc concentrations in 20 mM NaP_i and 100 mM NaCl (pH 6.0) at 22 °C. The data for the wt CcP (●), MH$_6$KT CcP (○), and CcP(His)$_6$ (★) were fit to eq 3 (—). See Table 4 and the text for details.

active. The concentration dependence of the initial velocities (v_0/e) for MH$_6$KT CcP is similar to that of the wt enzyme, while that of CcP(His)$_6$, showing saturation at lower Cc concentrations, appears to be different (Figure 7).

CpdI reduction by hCc is a complex phenomenon. As a rule, steady-state kinetics exhibit biphasic behavior, with the relative contributions of the two phases depending on the experimental conditions.[1] Here, we fit the data to three models (eq 3 in Materials and Methods): a simple Michaelis−Menten kinetics (MMK; model 1), MMK with a term incorporating linear $v_0/e = f([Cc])$ dependence (model 2), and biphasic kinetics

dx.doi.org/10.1021/bi400220w | Biochemistry 2013, 52, 2165−2175

described by a sum of two MMK terms (model 3). The model selection was performed using F statistics.[40] We found that model 1 adequately described the steady-state reduction of the wt and MH_6KT CpdI, and inclusion of additional parameters (i.e., models 2 and 3) did not lead to a statistically significant increase in the fit quality. In contrast, $CcP(His)_6$ kinetics could be described much better by model 2. Comparison of the determined $F(1,10) = 21.0$ to the theoretical $F_{0.01}(1,10) = 5.0$ suggests that model 2 fits the data better than model 1 with 99% probability. Inclusion of an extra parameter (i.e., model 3) does not significantly improve the fit compared to that of model 2. The kinetic parameters determined for each CcP construct are listed in Table 4. It should be noted that, over a broad range of experimental conditions, K_{M1} values for CpdI reduction by hCc do not correlate with the equilibrium dissociation constant (K_D) of the CcP–hCc complex[1] and, thus, cannot be used as a measure of the Cc binding affinity.

Table 4. Steady-State Kinetic Parameters for hCc Oxidation by CcP CpdI in 20 mM NaP_i and 100 mM NaCl (pH 6.0) at 22 °C As Determined by eq 3 (Materials and Methods)[a]

construct	model	K_{M1} (μM)	V_1/e (s^{-1})	V_2/eK_{M2} (s^{-1} μM^{-1})
wt CcP	1	10.0 ± 1.5	149.4 ± 5.4	
MH_6KT CcP	1	29.0 ± 4.0	172.5 ± 9.0	
$CcP(His)_6$	2	1.22 ± 0.73	24.6 ± 2.3	0.30 ± 0.04

[a]For the definition of the models and kinetic parameters, see Materials and Methods.

Cc Binding. The Cc binding properties of different CcP constructs were investigated by NMR spectroscopy. Incremental addition of increasing amounts of yCc to a CcP solution leads to a systematic shift in the position of the well-resolved, hyperfine-shifted Cc heme 3-CH_3 resonance in the 1D ^1H NMR spectrum.[41] The resulting plots of the observed binding shifts versus the ratio of protein concentrations (Figure 8) can be used to derive K_D values for the CcP–Cc complexes.[25] For the wt CcP–Cc, the K_D of 5.5 ± 0.5 μM obtained in this work agrees closely with the literature K_D value of 5 μM determined under the same solution conditions.[7,25] The MH_6KT CcP–Cc titration profile is highly similar to that of the wt complex (compare panels A and B of Figure 8), with the K_D values being the same within experimental error, suggesting that introduction of the N-terminal His tag does not perturb the interaction of CcP with yCc. In contrast, a ~55-fold decrease in binding affinity is observed for the $CcP(His)_6$–yCc system compared to that of the wt complex (Figure 8C). Such decrease in affinity is consistent with the CcP–yCc X-ray structure,[42] where the binding interface encompasses the C-terminal CcP region, and suggests that the C-terminal His tag interferes with Cc association. It is conceivable that impaired binding of Cc to the high-affinity crystallographic site shifts the interaction equilibrium toward a distant, functional, low-affinity site,[1,6] which could explain the peculiar concentration dependence of the steady-state kinetics (see above). If this is indeed the case, then the $CcP(His)_6$ construct could facilitate structural characterization of Cc binding to the low-affinity site.

Concluding Remarks. Using a high-yield expression system in *E. coli*, we produced both native and His-tagged CcP constructs either at natural abundance or as isotopically enriched, highly perdeuterated proteins. The engineered His tag greatly simplifies the CcP purification procedure and increases its solubility, allowing preparation of concentrated, stable NMR samples, which provided nearly complete backbone resonance assignments. We demonstrated that the introduction of the His tag at either the N-terminus or the C-terminus does not perturb the structure of the enzyme or alter the heme environment and ligand binding properties. Both constructs remained catalytically active yet exhibited differences in Cc binding, most likely because of steric occlusion of the high-affinity site by the C-terminal His tag. The availability of the resonance assignments for the CcP constructs with the N- or C-terminal His tag opens a way to study binding of Cc to the high- or low-affinity sites, respectively, by heteronuclear solution NMR spectroscopy.

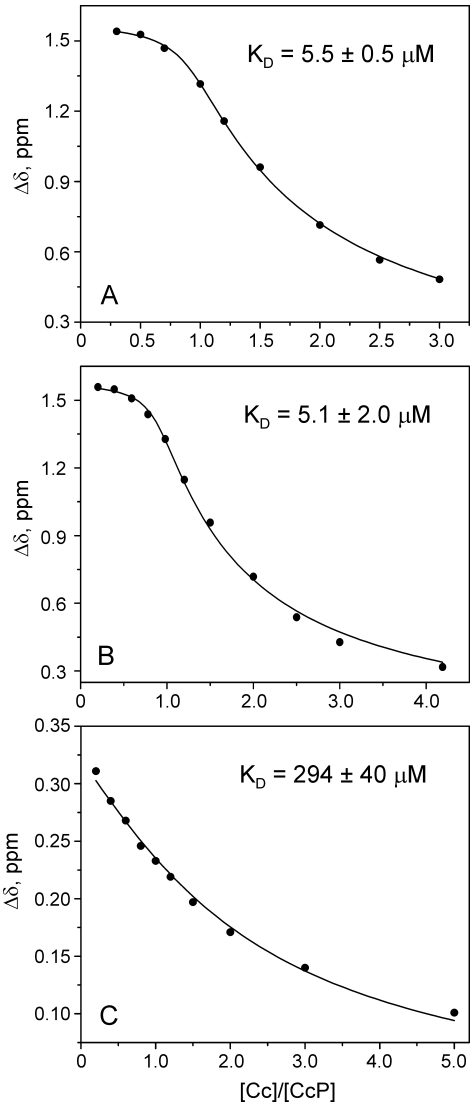

Figure 8. Chemical shift perturbations ($\Delta\delta$) of the 3-CH_3 heme resonance of the ferric yCc upon binding to the resting-state CcP. Binding to (A) wt CcP, (B) MH_6KT CcP, and (C) $CcP(His)_6$ in 20 mM NaP_i and 100 mM NaCl (pH 6.0) at 303 K. The solid lines show the best fit of the data to the binding curve (eq 2). Values of the equilibrium dissociation constants are indicated.

■ ASSOCIATED CONTENT

Supporting Information

CcP expression plasmid map, SDS–PAGE analysis of protein expression and solubility, UV–vis and CD spectra of the His-

tagged CcP constructs, $^{1}H-^{13}C$ planes of the triple-resonance NMR spectra, assigned HSQC spectra of both His-tagged CcP constructs, the assignment extent graph for MH_6KT CcP-CN, the plot of chemical shift differences between C- and N-terminally His-tagged CcP constructs, a table of X-ray data collection and refinement statistics, and supplementary references. This material is available free of charge via the Internet at http://pubs.acs.org.

AUTHOR INFORMATION

Corresponding Author

*E-mail: ovolkov@vub.ac.be. Telephone: (+32) 2 629 1025. Fax: (+32) 2 629 1963.

Funding

A.N.V. is an FWO Post-Doctoral Researcher. We acknowledge financial support from VIB and the Hercules Foundation. N.A.J.v.N. is a VIB group leader.

Notes

The authors declare no competing financial interest.

ACKNOWLEDGMENTS

We thank Didier Vertommen for mass spectrometric analysis and Sophie Vanwetswinkel and Yann Sterckx for critical reading of the manuscript.

ABBREVIATIONS

Cc, cytochrome *c*; CcP, yeast cytochrome *c* peroxidase; CD, circular dichroism; CpdI, Compound I; DLS, dynamic light scattering; ET, electron transfer; hCc, horse cytochrome *c*; HSQC, heteronuclear single-quantum coherence; LB, Luria-Bertani medium; MM, minimal medium; MMK, Michaelis–Menten kinetics; PEG, polyethylene glycol; SB, Super Broth; TB, Terrific Broth; yCc, yeast iso-1-cytochrome *c*.

REFERENCES

(1) Erman, J. E., and Vitello, L. B. (2002) Yeast cytochrome *c* peroxidase: Mechanistic studies via protein engineering. *Biochim. Biophys. Acta 1597*, 193–220.

(2) Altschul, A. M., Abrams, R., and Hogness, T. R. (1939) Soluble cytochrome *c* oxidase. *J. Biol. Chem. 130*, 427–428.

(3) Altschul, A. M., Abrams, R., and Hogness, T. R. (1940) Cytochrome *c* peroxidase. *J. Biol. Chem. 136*, 777–794.

(4) Stemp, E. D. A., and Hoffman, B. M. (1993) Cytochrome *c* peroxidase binds two molecules of cytochrome *c*: Evidence for a low-affinity, electron-transfer-active site on cytochrome *c* peroxidase. *Biochemistry 32*, 10848–10865.

(5) Zhou, J. S., and Hoffman, B. M. (1994) Stern-Volmer in reverse: 2:1 stoichiometry of the cytochrome *c*-cytochrome *c* peroxidase electron-transfer complex. *Science 265*, 1693–1696.

(6) Volkov, A. N., Nicholls, P., and Worrall, J. A. R. (2011) The complex of cytochrome *c* and cytochrome *c* peroxidase: The end of the road? *Biochim. Biophys. Acta 1807*, 1482–1503.

(7) Worrall, J. A. R., Kolczak, U., Canters, G. W., and Ubbink, M. (2001) Interaction of yeast *iso*-1-cytochrome *c* with cytochrome *c* peroxidase investigated by [^{15}N, ^{1}H] heteronuclear NMR spectroscopy. *Biochemistry 40*, 7069–7076.

(8) Volkov, A. N., Worrall, J. A. R., Holtzmann, E., and Ubbink, M. (2006) Solution structure and dynamics of the complex between cytochrome *c* and cytochrome *c* peroxidase determined by paramagnetic NMR. *Proc. Natl. Acad. Sci. U.S.A. 103*, 18945–18950.

(9) Volkov, A. N., Ubbink, M., and van Nuland, N. A. J. (2010) Mapping the encounter state of a transient protein complex by PRE NMR spectroscopy. *J. Biomol. NMR 48*, 225–236.

(10) Yonetani, T. (1967) Studies on cytochrome *c* peroxidase: X. Crystalline apo- and reconstituted holoenzymes. *J. Biol. Chem. 242*, 5008–5013.

(11) Fishel, L. A., Villafranca, J. E., Mauro, J. M., and Kraut, J. (1987) Yeast cytochrome *c* peroxidase: Mutagenesis and expression in *Escherichia coli* show tryptophan-51 is not the radical site in compound I. *Biochemistry 26*, 351–360.

(12) Goodin, D. B., Davidson, M. G., Roe, J. A., Mauk, A. G., and Smith, M. (1991) Amino acid substitutions at tryptophan-51 of cytochrome *c* peroxidase: Effects on coordination, species preference for cytochrome *c*, and electron transfer. *Biochemistry 30*, 4953–4962.

(13) Teske, J. G., Savenkova, M. I., Mauro, J. M., Erman, J. E., and Satterlee, J. D. (2000) Yeast cytochrome *c* peroxidase expression in *Escherichia coli* and rapid isolation of various highly pure holoenzymes. *Protein Expression Purif. 19*, 139–147.

(14) Weiner, M. P., Costa, G. L., Schoettlin, W., Cline, J., Mathur, E., and Bauer, J. C. (1994) Site-directed mutagenesis of double-stranded DNA by the polymerase chain reaction. *Gene 151*, 119–123.

(15) Savenkova, M. I., Satterlee, J. D., Erman, J. E., Siems, W. F., and Helms, G. L. (2001) Expression, purification, characterization, and NMR studies of highly deuterated recombinant cytochrome *c* peroxidase. *Biochemistry 40*, 12123–12131.

(16) Volkov, A. N., Vanwetswinkel, S., Van de Water, K., and van Nuland, N. A. J. (2012) Redox-dependent conformational changes in eukaryotic cytochromes revealed by paramagnetic NMR spectroscopy. *J. Biomol. NMR 52*, 245–256.

(17) Erman, J. E. (1974) Kinetic and equilibrium studies of cyanide binding by cytochrome *c* peroxidase. *Biochemistry 13*, 39–45.

(18) Otwinowski, Z., and Minor, W. (1997) Processing of X-ray diffraction data collected in oscillation mode. *Methods Enzymol. 276*, 307–326.

(19) Bonagura, C. A., Bhaskar, B., Shimizu, H., Li, H., Sundaramoorthy, M., McRee, D. E., Goodin, D. B., and Poulos, T. L. (2003) High-resolution crystal structures and spectroscopy of native and compound I cytochrome *c* peroxidase. *Biochemistry 42*, 5600–5608.

(20) Emsley, P., and Cowtan, K. (2004) Coot: Model-building tools for molecular graphics. *Acta Crystallogr. D60*, 2126–2132.

(21) Murshudov, G. N., Vagin, A. A., and Dodson, E. J. (1997) Refinement of macromolecular structures by the maximum-likelihood method. *Acta Crystallogr. D53*, 240–255.

(22) Laskowski, R. A., MacArthur, M. W., Moss, D. S., and Thornton, J. M. (1993) PROCHECK: A program to check the stereochemical quality of protein structures. *J. Appl. Crystallogr. 26*, 283–291.

(23) Delaglio, F., Grzesiek, S., Vuister, G. W., Zhu, G., Pfeifer, J., and Bax, A. (1995) NMRPipe: A multidimensional spectral processing system based on UNIX pipes. *J. Biomol. NMR 6*, 277–293.

(24) Vranken, W. F., Boucher, W., Stevens, T. J., Fogh, R. H., Pajon, A., Llinas, M., Ulrich, E. L., Markley, J. L., Ionides, J., and Laue, E. D. (2005) The CCPN data model for NMR spectroscopy: Development of a software pipeline. *Proteins 59*, 687–696.

(25) Volkov, A. N., Bashir, Q., Worrall, J. A. R., and Ubbink, M. (2009) Binding hot spot in the weak protein complex of physiological redox partners yeast cytochrome *c* and cytochrome *c* peroxidase. *J. Mol. Biol. 385*, 1003–1013.

(26) Kang, D. S., and Erman, J. E. (1982) The cytochrome *c* peroxidase-catalyzed oxidation of ferrocytochrome *c* by hydrogen peroxide. Steady state kinetic mechanism. *J. Biol. Chem. 257*, 12775–12779.

(27) Matthis, A. L., and Erman, J. E. (1995) Cytochrome *c* peroxidase-catalyzed oxidation of yeast *iso*-1 ferrocytochrome *c* by hydrogen peroxide. Ionic strength dependence of the steady-state parameters. *Biochemistry 34*, 9985–9990.

(28) Kim, K. L., Kang, D. S., Vitello, L. B., and Erman, J. E. (1990) Cytochrome *c* peroxidase catalyzed oxidation of ferrocytochrome *c* by hydrogen peroxide: Ionic strength dependence of the steady-state parameters. *Biochemistry 29*, 9150–9159.

(29) Yonetani, T., and Ray, G. S. (1965) Studies on cytochrome *c* peroxidase: I. Purification and some properties. *J. Biol. Chem. 240*, 4503−4508.
(30) Iizuka, T., Kotani, M., and Yonetani, T. (1971) Magetic susceptibility measurements of cytochrome *c* peroxidase and its complexes. *J. Biol. Chem. 246*, 4731−4736.
(31) DeLauder, S. F., Mauro, J. M., Poulos, T. L., Williams, J. C., and Schwarz, F. P. (1994) Thermodynamics of hydrogen cyanide and hydrogen fluoride binding to cytochrome *c* peroxidase and its Asn-82 → Asp mutant. *Biochem. J. 302*, 437−442.
(32) Erman, J. E. (1974) Kinetic studies of fluoride binding by cytochrome *c* peroxidase. *Biochemistry 13*, 34−39.
(33) Neri, F., Kok, D., Miller, M. A., and Smulevich, G. (1997) Fluoride binding in hemoproteins: The importance of the distal cavity structure. *Biochemistry 36*, 8947−8953.
(34) Sievers, G. (1978) Circular dichroism studies on cytochrome *c* peroxidase from baker's yeast (*Saccharomyces cerevisiae*). *Biochim. Biophys. Acta 536*, 212−225.
(35) Edwards, S. L., Poulos, T. L., and Kraut, J. (1984) The crystal structure of fluoride-inhibited cytochrome *c* peroxidase. *J. Biol. Chem. 259*, 12984−12988.
(36) Edwards, S. L., and Poulos, T. L. (1990) Ligand binding and structural perturbations in cytochrome *c* peroxidase. *J. Biol. Chem. 265*, 2588−2595.
(37) Satterlee, J. D., and Erman, J. E. (1981) Proton nuclear magnetic resonance characterization of the oxidized intermediates of cytochrome *c* peroxidase. *J. Biol. Chem. 256*, 1091−1093.
(38) Satterlee, J. D., and Erman, J. E. (1983) Deuterium exchangeable proton hyperfine resonances of low-spin cytochrome *c* peroxidase and the mechanism of peroxidase catalysis. *Biochim. Biophys. Acta 743*, 149−154.
(39) Gardner, K. H., and Kay, L. E. (1998) The use of ^{2}H, ^{13}C, ^{15}N multidimensional NMR to study the structure and dynamics of proteins. *Annu. Rev. Biophys. Biomol. Struct. 27*, 357−406.
(40) Bevington, P. R., and Robinson, D. K. (2003) *Data reduction and error analysis for the physical sciences*, 3rd ed., McGraw-Hill, Boston.
(41) Satterlee, J. D., Moench, S. J., and Erman, J. E. (1987) A proton NMR study of the non-covalent complex of horse cytochrome *c* and yeast cytochrome-*c* peroxidase and its comparison with other interacting protein complexes. *Biochim. Biophys. Acta 912*, 87−97.
(42) Pelletier, H., and Kraut, J. (1992) Crystal structure of a complex between electron transfer partners, cytochrome *c* peroxidase and cytochrome *c*. *Science 258*, 1748−1755.
(43) Yonetani, T., and Anni, H. (1987) Yeast cytochrome *c* peroxidase. Coordination and spin states of heme prosthetic group. *J. Biol. Chem. 262*, 9547−9554.
(44) Cheung, M. S., Maguire, M. L., Stevens, T. J., and Broadhurst, R. W. (2010) DANGLE: A Bayesian inferential method for predicting protein backbone dihedral angles and secondary structure. *J. Magn. Reson. 202*, 223−233.